Appl Phys B (2009) 97: 35–46
DOI 10.1007/s00340-009-3463-6

Applied Physics B
Lasers and Optics

Frequency-modulation spectroscopy of coherent dark resonances in ^{87}Rb atoms

Y.V. Vladimirova · V.N. Zadkov · A.V. Akimov · A.Y. Samokotin · A.V. Sokolov · V.N. Sorokin · N.N. Kolachevsky

Received: 6 February 2009 / Published online: 3 April 2009

Abstract The results of frequency-modulation (FM) spectroscopy of coherent dark resonances from the Zeeman sublevels of the transition $F = 2 \leftrightarrow F = 1$ of D_1 line in absorption of ^{87}Rb atoms are presented and discussed in detail. By contrast with the conventional spectroscopy of coherent dark resonances employing two laser beams, relative frequency of which can be varied, these data has been obtained with the help of a single frequency-modulated laser field. Variation of the modulation frequency plays then a similar role as the variation of the relative frequency in conventional spectroscopy. Experimental data are fit to the theoretical calculations, which are based on the theory of FM spectroscopy of coherent dark resonances recently developed by us. Feasibility of using such experimental technique for accurate measurements of magnetic fields is also discussed.

PACS 42.50.Hz · 42.50.Gy · 32.70.Jz · 32.10.Dk

Y.V. Vladimirova · V.N. Zadkov (✉)
International Laser Center and Faculty of Physics,
M.V. Lomonosov Moscow State University, Moscow 119991, Russia
e-mail: zadkov@phys.msu.ru

Y.V. Vladimirova
e-mail: vladimirova@phys.msu.ru

A.V. Akimov · A.Y. Samokotin · A.V. Sokolov · V.N. Sorokin · N.N. Kolachevsky
P.N. Lebedev Physical Institute, Russian Academy of Sciences, Leninski ave. 53, Moscow 119991, Russia

A.V. Akimov · A.Y. Samokotin · A.V. Sokolov · V.N. Sorokin · N.N. Kolachevsky
Moscow Institute of Physics and Technology, Dolgoprudny 141700, Moscow Region, Russia

1 Introduction

The coherent population trapping (CPT) is one of the most intriguing quantum interference phenomena that can be most vividly seen in a three-level system in Λ-configuration. In this system, if two monochromatic pumping fields are tuned into the resonance with the respective transitions, all the population is captured in the coherent superposition of two low-lying levels, which gives the name of the phenomenon—coherent population trapping [1]. This means that the media of such three-level atoms under CPT will not emit fluorescence and do not absorb photons. In absorption spectra, it is revealed as a narrow sharp dip in the absorption profile while scanning frequency of one of the pumping laser fields. These resonances are called the coherent dark resonances. Due to the rather small spectral width of the dark resonances, they found applications in precision spectroscopic applications, such as metrology [1], magnetometry [2], and highly-sensitive laser interferometers for registration of gravitational waves [3]. CPT phenomenon lies also in the foundation of the lasers without inversion [4]. CPT is also widely used in research related to cooling of atoms and molecules [5] and optical bistability, as well as in research on engineering of quantum states, in quantum information, and in quantum communication (see, for instance, [6, 7]). Among all these applications are the feasibility studies of using the coherent dark resonances spectroscopy in a vapor of alkali atoms as a prototype of the sensitive magnetometers. Alkali-based optical magnetometers are widely used now for precision measurement of the magnetic fields in a wide dynamical range (up to mT) and provide sensitivity on the level of a few fractions of nT (see, for instance, [8]). Such magnetometers can also be used for measurements of the magnetic field of the Earth, laboratory

fields, fields in the medicine including performance of optical magnetic cardiography [9] and in a number of important fundamental research projects (i.e., in experiments on the search of an electrical dipole moment of a neutron [10]).

Along with conventional spectroscopy of coherent dark resonances, which employ two laser fields, one can use also FM-spectroscopy that employs interaction of the atomic system with single frequency modulated laser field. Optical FM spectroscopy, which methods started to be developed in the beginning of 1980s, plays nowadays one of the central roles in high-precision measurements in such fields of physics as detecting the gravitational waves, frequency standards, measuring of the weak magnetic fields, etc. (see the review [11]). Despite significant progress in development of optical FM-spectroscopy techniques, theoretical models were elaborated and studied in detail only for the two-level systems, which allow analytical solutions. Even interaction of a three-level system with FM laser field was not considered theoretically till our recent works [12, 13], though interaction of such systems with bichromatic laser radiation has been studied in detail. In magnetic fields, situation is even more complicated because the atomic structure significantly enriches due to the lifting of the degeneracy of the atomic levels. This require special theoretical consideration. On experimental side, there is only one publication of the experimental results on the FM spectroscopy of coherent dark resonance in a vapor of Cs atoms [14]. However, detailed comparison of the experimental data published in this work and theoretical calculations is not feasible because the authors determined the FM index indirectly, from analysis of the spectra of coherent dark resonances themselves.

In this work, we made a detailed analysis and comparison of experimental data obtained with the FM laser spectroscopy for the D_1 line in ^{87}Rb atoms and theoretical calculations based on the model described in [12, 13]. For this, our simple model was extended on the case of a real multilevel atom. In experiment, we measured dark resonances at the Zeeman sublevels of the transition $5^2S_{1/2}(F=2) \leftrightarrow 5^2P_{1/2}(F=1)$ in transmission spectra in the constant magnetic field. Simultaneously, the FM index was measured with the help of Fabri–Perot interferometer. FM spectra are registered either (i) by scanning the modulation frequency at the fixed magnetic field or (ii) by scanning the strength of the magnetic field at the fixed modulation frequency. Spectra obtained both these ways are in a good agreement with the theoretical model. Feasibility of using FM spectroscopy of dark resonances for optical magnetometry is also discussed. The estimated resolution for measuring a magnetic field B in the range 10 G to 100 G is equal to $\sigma_B/B \approx 7 \times 10^{-6}$ for the measuring time $\tau = 3$ ms in a cell of Rb atoms with a buffer gas. We also evaluate a working range for the magnetometer.

The paper is organized as follows. In Sect. 2, we briefly outline the basics of the coherent population trapping phenomenon. Section 3 defines the basics of the FM spectroscopy of the coherent dark resonances, theoretical model of which is discussed in Sect. 4. Experimental part of the work is described in Sect. 5, whereas theoretical modeling of obtained in experiment spectra and their detailed comparison are given in Sect. 6. Feasibility of using FM spectroscopy of coherent dark resonances for magnetometry is discussed in Sect. 7. In conclusion, we summarize key results of our work.

2 Coherent population trapping phenomenon

The coherent population trapping phenomenon (CPT) can be most vividly seen in a three-level system in so called Λ-configuration (Fig. 1), which contains of two low-lying long-lived levels $|1\rangle$ and $|2\rangle$, dipole transition between which is strongly forbidden, and a third distant level $|3\rangle$, which is coupled with the two others by two cw laser fields.

Let us assume that the transition $|1\rangle \leftrightarrow |2\rangle$ is strictly forbidden in dipole approximation and two monochromatic pumping fields $E_1 \exp(-i\omega_{L1}t - i\varphi_1)$, $E_2 \exp(-i\omega_{L2}t - i\varphi_2)$ are tuned into the resonance with the respective transitions $|1\rangle \leftrightarrow |3\rangle$, $|2\rangle \leftrightarrow |3\rangle$. Due to the quantum interference at the zero Raman detuning $\delta_R = \omega_{L1} - \omega_{L2} - \omega_{12}$ all the population in the Λ-system is captured in the coherent superposition of two low-lying levels [15, 16]. This means that the media of such three-level atoms under CPT-condition will not emit fluorescence (because the population of the excited state goes to zero under the CPT and the fluorescence signal is proportional to it) and do not absorb photons, as well. Therefore, in absorption spectra, CPT is revealed as a narrow sharp dip in the absorption profile while

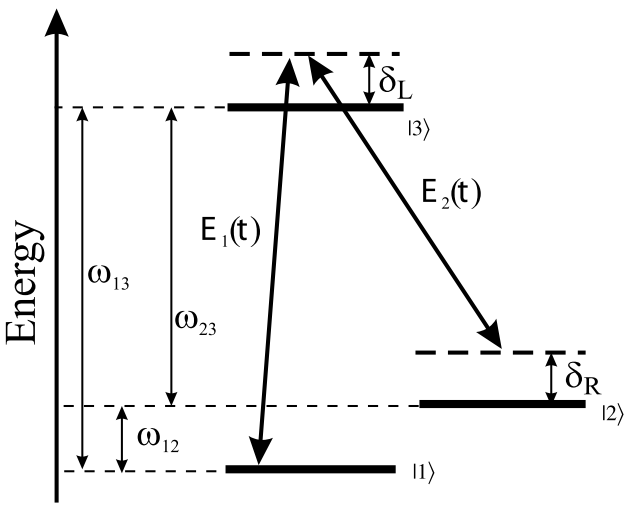

Fig. 1 Λ-system driven by two laser fields $E_1(t)$ and $E_2(t)$. Here δ_L is the one-photon laser detuning at the transition $|1\rangle \leftrightarrow |3\rangle$ and δ_R is the two-photon Raman detuning

scanning one of the pumping laser fields, for instance, with the frequency ω_{L1}. These resonances are called the coherent dark resonances as the media (atomic vapor) does not fluoresce under the CPT. Another side of the same phenomenon is that under the CPT the media shows so called electromagnetically-induced transparency (EIT) [17, 18]. For precision measurements it is important that the spectral width of these resonances is rather small and can achieve dozens of Hz in experiments with Cs atoms in a buffer gas at room temperature, see for instance, [19, 20].

In a simple three-level model that allows calculations in an analytical form, CPT phenomenon was understood and studied in detail in a review by Arimondo [16]. However, real atoms (especially in experiments with applied magnetic fields) are essentially multilevel systems and require therefore correct theoretical treatment beyond simple three-level approximation. In [21, 22], a specific case of alkali atoms in the limit of high buffer gas pressure, which allows to neglect the Doppler effect, was considered in detail. A universal theory, which allows correct description of N-level atom under any configurations of pumping electric and magnetic fields and takes into account the Doppler effect, has been suggested and verified by us earlier [23]. Here we will focus on a different experimental technique for registering spectra of the coherent dark resonances—FM spectroscopy. In the next section, we will consider how the coherent dark resonances are formed in the FM-spectroscopy on example of Rb atoms.

3 FM spectroscopy of coherent dark resonances in Rb atoms

By contrast with conventional spectroscopy of coherent dark resonances, which employ two laser fields, interaction of a three-level, for example Λ-system, with FM laser field essentially complicates the structure of the spectra leading to many additional resonances [12]. Besides that, complex Zeeman levels structure in real atoms significantly complicates the picture [23].

Talking of FM spectroscopy of coherent dark resonances, we need to distinguish between two different cases, *low*- and *high*-frequency modulation of the incident laser field.

The *low-frequency FM spectroscopy* is used in the case when FM-field excite only transitions from a single hyperfine sublevel, i.e., $F_g = 2$, where F is the quantum number of the entire atom's momentum. Here and further on, the lower indices g and e indicate that the value they stay at is related to the lower/upper levels of the transition, correspondingly. The resonance frequency is defined by the magnetic field and selected transition. For example, for the transition $F_g = 2 \rightarrow F_e = 1$ in D_1 line of ^{87}Rb (Fig. 2) and magnetic field strength of 10 G, the modulation frequency is about 14 MHz.

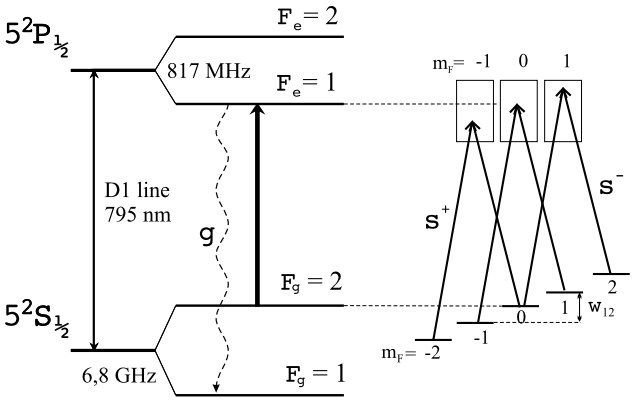

Fig. 2 Structure of the D_1 line in ^{87}Rb atom. The levels of the working transition $F_g = 2 \rightarrow F_e = 1$ are split in the applied magnetic field into $2F + 1$ sublevels each. The pairs of Zeeman sublevels of the ground state $\Delta m_F = 2$ and those of excited state form a chain of three Λ-systems

The *high-frequency FM spectroscopy* is used for excitation the dark resonances at simultaneous excitation of two hyperfine sublevels $F_g = 1$ and $F_g = 2$. Frequency modulation in this case is equal to the half of the hyperfine splitting value, i.e., approximately 3.4 GHz for Rb atom.

Therefore, one can consider two different configurations for FM spectroscopy of the dark resonances:

- *Dark resonances at the Zeeman sublevels of the ground state*, where $|1\rangle$ and $|2\rangle$ are the Zeeman sublevels of the same hyperfine ground component. In the case when laser field is linearly polarized, transitions from levels $|1\rangle = |F_g, m_F\rangle$ and $|2\rangle = |F_g, (m_F + 2)\rangle$ onto the excited level $|3\rangle = |F_e, (m_F + 1)\rangle$ are possible, where $F_g = 2$ and $F_e = 1$ (see, e.g., [24]);
- *Dark resonances at the levels of the hyperfine structure of different ground states*, where $|1\rangle$ and $|2\rangle$ belong to two different hyperfine ground levels, so that $|1\rangle = |F_g = 1\rangle$ and $|2\rangle = |F_g = 2\rangle$. This case corresponds to the conventional spectroscopy of dark resonances in a Λ-system interacting with two pumping resonant fields (see, for instance, [14, 25]).

In this work, we focus at investigation of the interaction of FM laser field with a set of Zeeman sublevels in ^{87}Rb atom at transition $5S_{1/2}(F_g = 2) \rightarrow 5P_{1/2}(F_e = 1)$ (Fig. 2). This specific transition is chosen because the hyperfine sublevels of the excited level for this transition can be resolved in experiment on a Doppler-broadened profile, which allows investigation of this specific transition in a cell with atomic vapor at room temperature. Moreover, this transition ensures the highest contrast of the dark resonances at the Zeeman sublevels [26, 27].

Levels $F_g = 2$ and $F_e = 1$ are split in a magnetic field into $2F + 1$ sublevels each. Then, the pairs of Zeeman sublevels of the ground state $F_g = 2$ with $\Delta m_F = 2$ (m_F is the

magnetic quantum number) and those of the excited state $F_e = 1$ form a chain of three Λ-systems. In the following, we will assume that the atomic vapor is located in the *weak and homogeneous* magnetic field.

Modulation of the incident laser field is carried out by the modulation of the laser diode current at the frequency Ω_{mod}, which obviously leads to both amplitude modulation (AM) with the modulation index R and frequency modulation (FM) with the modulation index M. In the case of harmonic modulation, the incident laser field can be written as:

$$\begin{aligned} E(t) &= E_0\big[1 + R\sin(\Omega_{\text{mod}}t + \Psi)\big] \\ &\quad \times \exp\big[i(\omega_0 t + M\sin\Omega_{\text{mod}}t)\big] + \text{c.c.} \\ &= \frac{E_0}{2}\sum_{n=-\infty}^{+\infty} a_n \exp\big(i(\omega_0 + n\Omega_{\text{mod}})t\big) + \text{c.c.}, \end{aligned} \tag{1}$$

where Ψ is the relative phase between the frequency and amplitude modulation and coefficients a_n in the Fourier series are expressed via the Bessel functions $J_n(M)$ as

$$a_n = J_n(M) - i\frac{R}{2}J_{n-1}(M)e^{i\Psi} + i\frac{R}{2}J_{n+1}(M)e^{-i\Psi}. \tag{2}$$

The incident laser field spectrum is modified when the modulation index M and/or the modulation frequency Ω_{mod} is changed. When Ω_{mod} is fixed, increasing the modulation index leads to the increase of the number of resonances in the resulting spectrum, which are separated by Ω_{mod} [12].

Due to the interaction of the Λ-system with the FM-field each pair of the field spectrum components gives its own contribution to the dark resonance, which is formed when the frequency difference is coincide with the Zeeman splitting ω_{12} of the ground state, as it is shown in Fig. 3. Therefore, the spectrum is enriched with additional dark resonances called the high-order resonances. They will appear only if $\omega_{12} = k\Omega_{\text{mod}}$, where k is the order of the resonance

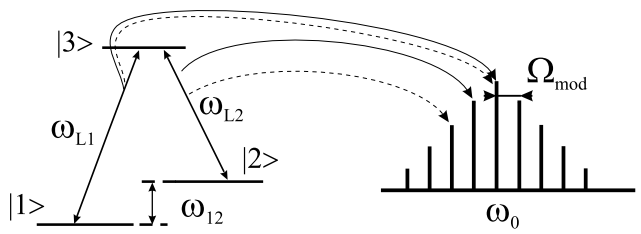

Fig. 3 Forming coherent dark resonances in case of Λ-system interacting with the FM laser field. All possible pairs of the field components take part in forming the resonance structure, out of which only two of them are show in the figure for simplicity. *Solid arrows* indicate two field components with the frequency difference Ω_{mod}, which take part in forming the dark resonance at the frequency Ω_{mod}, whereas *dashed arrows* indicate two field components with the frequency difference $2\Omega_{\text{mod}}$, which take part in forming the dark resonance at the frequency $2\Omega_{\text{mod}}$

(an integer number). Experimentally, dark resonances are observed either when one changes the modulation frequency at the fixed magnetic field magnitude or at the fixed modulation frequency by varying the magnetic field [12, 13].

As we mentioned earlier, modulation of the laser diode current causes both FM and AM of the incident laser field. The index of amplitude modulation R in our experiment does not exceed 0.025 (see Sect. 5). In this case, taking into account additional small amplitude modulation does not significantly change the structure of the dark resonances spectrum, slightly affecting the amplitudes of the resonances. From now on, when we talk of the FM field, we always assume that the amplitude modulation is also taken into account in all our calculations.

4 Theoretical model

4.1 Key equations

Temporal dynamics of a quantum system is governed by the following master equation:

$$\dot{\hat{\rho}} = -\frac{i}{\hbar}[\hat{H}, \hat{\rho}] + \mathcal{L}_{\text{relax}}\hat{\rho}, \tag{3}$$

where the first term in the right-side of the equation describes the reversible dynamics of the system with the Hamiltonian $\hat{H}$, and the second term describes non-reversible dynamics due to the stochastic interaction of the system with the reservoir, which is defined by the relaxation superoperator $\mathcal{L}_{\text{relax}}$. Under the assumption that the relaxation is Markovian, this superoperator can be represented in the form of averaged over the reservoir's noises $\hat{\xi}$ dynamics of the system–reservoir.

In a general form, the relaxation superoperator can be written as a sum of two terms:

$$\mathcal{L}_{\text{relax}} = \mathcal{L}_r + \mathcal{L}_e, \tag{4}$$

where $\mathcal{L}_r$ and $\mathcal{L}_e$ are the superoperators of radiative decay and of elastic dephasing, respectively.

The radiative decay superoperator has the form:

$$\mathcal{L}_r = \sum_{kl}\gamma_{kl}\left(\hat{P}_{lk}\odot\hat{P}_{kl} - \frac{1}{2}[\hat{P}_{kk}, \odot]_+\right), \tag{5}$$

where the two-dimensional array γ_{kl} contains the spontaneous decay velocities for $k > l$ and the pumping rates for $k < l$.

The elastic dephasing superoperator can be represented as the following sum:

$$\begin{aligned} \mathcal{L}_e &= \sum_{k<l}\big(\mathcal{L}_{\text{in}}^{kl} + \mathcal{L}_{\text{ex}}^{kl}\big) \\ &= -\Gamma_{\text{in}}^{kl}(\hat{P}_{kk}\odot\hat{P}_{ll} + \hat{P}_{ll}\odot\hat{P}_{kk}) - \Gamma_{\text{ex}}^{kl}[\hat{I}_{kl}, \odot]^2, \end{aligned} \tag{6}$$

where Γ_{in}^{kl} and Γ_{ex}^{kl} are the dephasing rates.

Solving the set of (3) for the specific problem, one can calculate, for instance, an absorbtion spectrum of the driven Λ-system.

Previously, we elaborated two methods for calculation of the temporal dynamics of the dark resonances spectrum formation and the resulting absorption spectrum [12, 13]. In this section, we will limit ourselves by considering a separate three-level Λ-system interacting with the incident FM laser field, as a model, in order to elucidate most essential features of this interaction. Further generalization of this model on a multilevel system, for instance, a chain of the Λ-systems forming by the Zeeman sublevels in applied magnetic field (Fig. 2), can be routinely done with the help of numerical modeling.

4.2 Absorption spectra calculation for a Λ-system interacting with the FM-field

The interaction Hamiltonian of the Λ-system with an incident FM laser field (1) has the form:

$$\hat{H} = \begin{pmatrix} 0 & 0 & e^{i\Delta(t)} g_{13}(1+\Delta'(t)) \\ 0 & -\omega_{12} & e^{i\Delta(t)} g_{23}(1+\Delta'(t)) \\ e^{-i\Delta(t)} g_{13}(1+\Delta'(t)) & e^{-i\Delta(t)} g_{23}(1+\Delta'(t)) & \delta_L \end{pmatrix}, \tag{7}$$

where $g_{k3} = -d_{k3}E_k/\hbar$ $(k = 1, 2)$ are the Rabi frequencies, determined through the corresponding dipole moments $d_{k3} = -e\langle k|r|3\rangle$; $\delta_L = \omega_0 - \omega_{13}$ is the one-photon detuning from the resonance, and ω_{12} is the frequency splitting of the ground state; $\Delta(t)$ and $\Delta'(t)$ are determined by the amplitude and frequency modulation, respectively:

$$\Delta(t) = M\sin(\Omega_{\text{mod}}t), \qquad \Delta'(t) = R\sin(\Omega_{\text{mod}}t). \tag{8}$$

Inserting the expression for $\mathcal{L}_{\text{relax}}(\rho)$ in the form of (4) into (3), we will have the following set of differential equations:

$$\begin{aligned}
\dot{\rho}_{11}(t) &= -\mu_{12}\rho_{11}(t) + \gamma_{21}\rho_{22}(t) \\
&\quad + i\big(e^{-i\Delta(t)} g_{13}\big(1+\Delta'(t)\big)\rho_{13}(t) \\
&\quad - e^{i\Delta(t)} g_{13}\big(1+\Delta'(t)\big)\rho_{31}(t)\big) + \gamma_{31}\rho_{33}(t), \\
\dot{\rho}_{12}(t) &= -\Gamma_{12}\rho_{12}(t) + i\big(-\omega_{12}\rho_{12}(t) \\
&\quad + e^{-i\Delta(t)} g_{23}\big(1+\Delta'(t)\big)\rho_{13}(t) \\
&\quad - e^{-i\Delta(t)} g_{13}\big(1+\Delta'(t)\big)\rho_{32}(t)\big), \\
\dot{\rho}_{13}(t) &= -\Gamma_{13}\rho_{13}(t) + i\big(e^{i\Delta(t)} g_{13}\big(1+\Delta'(t)\big)\rho_{11}(t) \\
&\quad + e^{i\Delta(t)} g_{23}\big(1+\Delta'(t)\big)\rho_{12}(t) \\
&\quad + \delta_L\rho_{13}(t) - e^{i\Delta(t)} g_{13}\big(1+\Delta'(t)\big)\rho_{33}(t)\big), \\
\dot{\rho}_{21}(t) &= -\Gamma_{21}\rho_{21}(t) + i\big(\omega_{12}\rho_{21}(t) \\
&\quad + e^{-i\Delta(t)} g_{13}\big(1+\Delta'(t)\big)\rho_{23}(t) \\
&\quad - e^{i\Delta(t)} g_{23}\big(1+\Delta'(t)\big)\rho_{31}(t)\big), \\
\dot{\rho}_{22}(t) &= \mu_{12}\rho_{11}(t) - \gamma_{21}\rho_{22}(t) \\
&\quad + i\big(e^{-i\Delta(t)} g_{23}\big(1+\Delta'(t)\big)\rho_{23}(t) \\
&\quad - e^{i\Delta(t)} g_{23}\big(1+\Delta'(t)\big)\rho_{32}(t)\big) + \gamma_{32}\rho_{33}(t),
\end{aligned} \tag{9}$$

$$\begin{aligned}
\dot{\rho}_{23}(t) &= -\Gamma_{23}\rho_{23}(t) + i\big(g_{13}\rho_{21}(t) \\
&\quad + e^{i\Delta(t)} g_{23}\big(1+\Delta'(t)\big)\rho_{22}(t) \\
&\quad + \delta_L\rho_{23}(t) + \omega_{12}\rho_{23}(t) \\
&\quad + e^{i\Delta(t)} g_{23}\big(1+\Delta'(t)\big)\rho_{33}(t)\big), \\
\dot{\rho}_{31}(t) &= -\Gamma_{31}\rho_{31}(t) + i\big(-e^{-i\Delta(t)} g_{13}\big(1+\Delta'(t)\big)\rho_{11}(t) \\
&\quad - e^{-i\Delta(t)} g_{23}\big(1+\Delta'(t)\big)\rho_{21}(t) \\
&\quad - \delta_L\rho_{31}(t) + e^{-i\Delta(t)} g_{13}\big(1+\Delta'(t)\big)\rho_{33}(t)\big), \\
\dot{\rho}_{32}(t) &= -\Gamma_{32}\rho_{32}(t) + i\big(-e^{-i\Delta(t)} g_{13}\big(1+\Delta'(t)\big)\rho_{12}(t) \\
&\quad - e^{-i\Delta(t)} g_{23}\big(1+\Delta'(t)\big)\rho_{22}(t) \\
&\quad - \delta_L\rho_{32}(t) - \omega_{12}\rho_{32}(t) \\
&\quad + e^{-i\Delta(t)} g_{23}\big(1+\Delta'(t)\big)\rho_{33}(t)\big), \\
\dot{\rho}_{33}(t) &= i\big(-e^{-i\Delta(t)} g_{13}\big(1+\Delta'(t)\big)\rho_{13}(t) \\
&\quad - e^{-i\Delta(t)} g_{23}\big(1+\Delta'(t)\big)\rho_{23}(t) \\
&\quad + e^{i\Delta(t)} g_{13}\big(1+\Delta'(t)\big)\rho_{31}(t) \\
&\quad + e^{i\Delta(t)} g_{23}\big(1+\Delta'(t)\big)\rho_{32}(t)\big) \\
&\quad - (\gamma_{31}+\gamma_{32})\rho_{33}(t),
\end{aligned}$$

where $\Gamma_{12} = \Gamma_{21} = 0.5(\gamma_{21} + \mu_{12})$, $\Gamma_{13} = \Gamma_{31} = 0.5(\gamma_{31} + \gamma_{32} + \mu_{12})$, $\Gamma_{23} = \Gamma_{32} = 0.5(\gamma_{21} + \gamma_{31} + \gamma_{32})$; γ_{31}, γ_{32}, and γ_{12} are the spontaneous decay rates, μ_{12} is the pumping rate of level $|2\rangle$. By solving this set of equations, one can calculate the temporal dependence of the excited state population $n_3(t)$ and the absorption spectrum of the driven Λ-system.

In reality, however, there exists an additional decay channel from level $5^2P_{1/2}$, $F_e = 1$ onto the level $5^2S_{1/2}$, $F_g = 1$, decay rate of which we will designate as γ (Fig. 2).

With this additional decay channel taken into account, our system becomes a four-level one. The Hamiltonian of such a system interacting with the FM-field has the form:

$$\hat{H} = \begin{pmatrix} 0 & 0 & 0 & e^{i\Delta(t)} g_{13}(1+\Delta'(t)) \\ 0 & -\omega_{12} & 0 & e^{i\Delta(t)} g_{23}(1+\Delta'(t)) \\ 0 & 0 & \delta_L & 0 \\ e^{-i\Delta(t)} g_{13}(1+\Delta'(t)) & e^{-i\Delta(t)} g_{23}(1+\Delta'(t)) & 0 & \delta'_L \end{pmatrix}, \tag{10}$$

$$L_{\text{relax}} = \begin{pmatrix} \gamma_{41}\rho_{44}(t) & 0 & 0 & \varkappa - \frac{\gamma_{43}}{2}\rho_{14}(t) \\ 0 & \gamma_{42}\rho_{44}(t) & 0 & \varkappa - \frac{\gamma_{43}}{2}\rho_{24}(t) \\ 0 & 0 & \gamma_{43}\rho_{44}(t) & 0 \\ \varkappa - \frac{\gamma_{43}}{2}\rho_{14}(t) & \varkappa - \frac{\gamma_{43}}{2}\rho_{24}(t) & 0 & -\gamma_{41} - \gamma_{42} - \gamma_{43}\rho_{44}(t) \end{pmatrix}, \tag{11}$$

where $\varkappa = -G - \frac{\gamma_{41}}{2} - \frac{\gamma_{42}}{2}$.

Substituting the expression for $\mathcal{L}_{\text{relax}}(\rho)$ in the form (11) into (3) with the Hamiltonian (10), we get a set of 16 differential equations. Calculated absorption spectra for the vapor of ^{87}Rb atoms are shown in Fig. 4 for different decay rates γ. These calculations have been made for $g_{12} = g_{13} = 1$ a.u., $M = 4$, $G = 10$ a.u., $\gamma_{31} = \gamma_{32} = 1$ a.u., and $\omega_{12}/2\pi = 20$ a.u., where a.u. = 1 MHz.

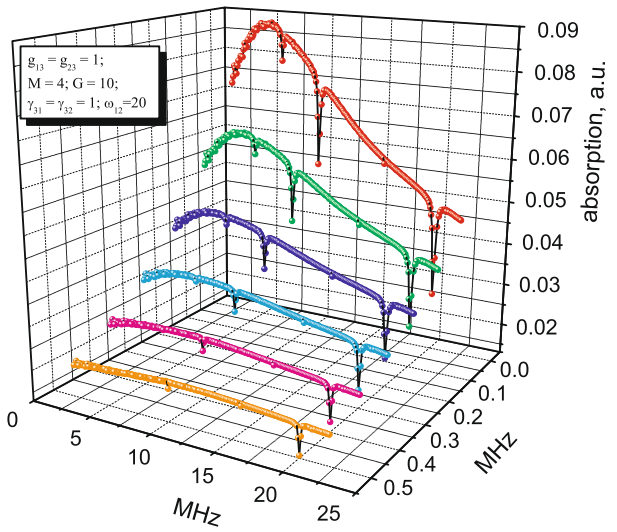

Fig. 4 Calculated absorption spectrum of FM laser light in a cell with Rb vapor versus the modulation frequency for different decay rates γ from level $5^2P_{1/2}$, $F = 2$ onto the level $5^2S_{1/2}$, $F = 1$ equal to 0, 0.1, 0.2, 0.3, 0.4, and 0.5

For convenience in further comparison with experimental data, Fig. 5 also shows the derivatives of the calculated absorption spectra with respect to the frequency Ω_{mod}. Shown dependencies demonstrate that the overall absorption is reduced and relationship between the amplitudes of the resonances is changed with increasing the decay rate. For example, at $\gamma = 0$ (Fig. 5) the relationship of the amplitudes of the resonances at the frequencies $\Omega_{\text{mod}} = \omega_{12}$ and $\Omega_{\text{mod}} = \omega_{12}/2$ is approximately equal to 1:1, whereas at $\gamma = 0.5$ (Fig. 5) it corresponds to 3:1.

5 Experimental setup for the FM spectroscopy of coherent dark resonances

An experimental setup for FM spectroscopy of coherent dark resonances is shown in Fig. 6 [28]. Laser radiation from a diode laser with an external resonator ($\lambda = 795$ nm) assembled by Littrow scheme is frequency modulated by modulation of the laser diode current. A frequency synthesizer SML-03 (Rohde&Schwarz) serves as the radio-frequency oscillator, which modulates laser frequency in the range $\Omega_{\text{mod}} = (2\text{–}100)$ MHz. Modulation index can be varied by

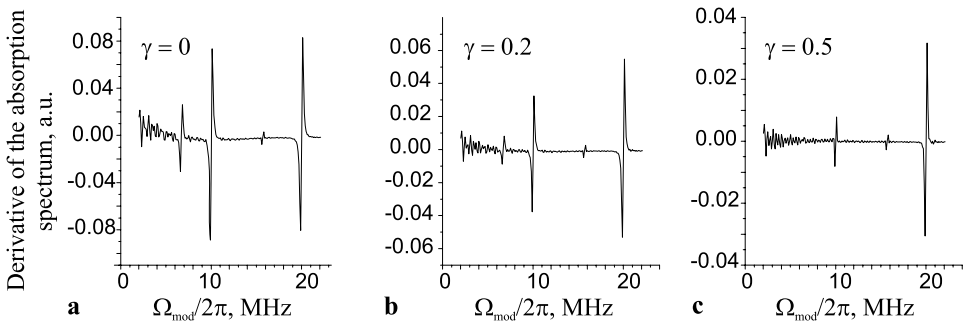

Fig. 5 Derivative of the absorption spectra shown in Fig. 4 with respect to the frequency Ω_{mod}

varying the level of the oscillator's signal. Laser beam passes then through the optical isolator and guides to the sample cell with the help of a single-mode optical fiber, which forms the Gaussian spatial mode of the radiation with diameter 4.5 mm at the level $1/e$. Part of the laser beam is also used for controlling the wavelength and mode composition of the radiation by a wavemeter and a scanning interferometer (a free spectral range $R = 630$ MHz, finesse $\mathcal{F} \simeq 10$). This interferometer does not allow resolving the spectral components of the FM-spectrum, however, gives a rough estimate of the modulation index from the broadening of the transmission peaks.

Besides this rough estimate of the modulation index, we also measured it with the help of a high-resolution interferometer. For this, the light was guided by the optical fiber in a more high-Q Fabri–Perot interferometer (length is about 50 cm, the input mirror is a plain one, the output mirror is the concave one with the radius 1 m) (Fig. 6). The interferometer ($R = 300$ MHz and $\mathcal{F} \simeq 400$) allows registration of the FM light spectrum with resolution of about 1 MHz. In order to obtain spectrum of the laser field, one has to apply a periodical saw-toothed signal at the piezoceramic plate controlling position of the diffraction grating of the external laser resonator. This leads to the periodical, linear in time variation of the laser frequency generation.[1] The photodiode at the exit from interferometer measured the transmitted light power. The registered dependency of the photodiode voltage vs time reflects the dependency of the intensities of the different modes in the FM-spectrum from their frequencies.

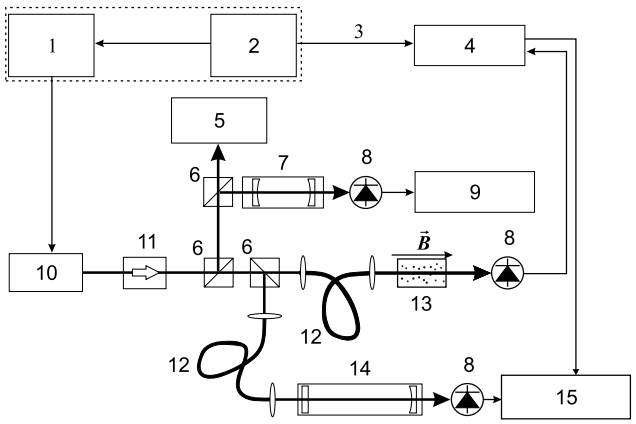

Fig. 6 Scheme of experimental setup: high-frequency generator (*1*), low-frequency generator (*2*), reference signal (*3*), lock-in detector (*4*), lambda-meter (*5*), polarization beamsplitters (*6*), scanning interferometer (*7*), photodiodes (*8*), digital oscilloscope (*9*), semiconductor laser with external cavity (*10*), optical isolator (*11*), optical fiber (*12*), cell with Rb vapor (*13*), interferometer (*14*), personal computer (*15*). Half-wave plates in front of the polarization beamsplitters 6 are not shown

[1]Note that during measurement of the FM index M we stop registration of the coherent dark resonances spectrum.

For the measured experimentally spectrum, we then fit the value of M at which the calculated spectrum has the same intensities relation as in the experimental spectrum.

Examples of both experimental and calculated FM spectra for various values of M are given in Fig. 7. Direct measurements of the laser diode radiation dependency versus time with the help of a photodiode with the frequency range 200 MHz show that the amplitude modulation index R does not exceed the value of 0.025. Therefore, as we stated before, the additional amplitude modulation just insignificantly affects the amplitudes of the coherent dark resonances.

It is worth to note that at the constant voltage at the generator, which modulates the laser diode current, FM index depends on the modulation frequency. Typical dependence is shown in Fig. 8. Sharp growth of M at the modulation frequency below 20 MHz is most probably due to the existence of the resonance in a laser diode current circuit. Solid line in the figure corresponds to the fit with the following approximation function:

$$M = A/\left[\Omega_{\text{mod}}/(2\pi \times 1\ \text{MHz})\right]^B, \tag{12}$$

where A and B are the approximation parameters.

In an applied magnetic field, upper and low levels of the considered transition in Rb are split into 3 and 5 magnetic sublevels, respectively (see Fig. 2). In the case of a weak magnetic field, optical field is still in resonance with the one-photon atomic transitions for all values of magnetic quantum numbers m_F and splitting of the upper level plays no essential role in forming the CPT states, whereas splitting of the lower level leads to the forming of three Λ-systems. In the case of the linear Zeeman effect, splitting of the lower levels for all three systems is the same, and only one resonance is observed in the experiment. By increasing the intensity of the magnetic field, quadratic Zeeman effect comes into play and leads to the broadening and then to the splitting of this resonance into three [29].

The sample cell with the vapor of Rb atoms is located along the solenoid axis, the latter supplied with additional winding at the edges for improving the field homogeneity. The solenoid itself is located under the two-layer magnetic insulation. The latter ensures the residual field at the level less than 10 mG. Intensity of the light transmitted through the cell is registered by a photodiode. The cell can be heated within the range of 30–70°C to ensure an essential absorption at the resonance line.

In order to raise the signal to noise ratio at the registration of the dark resonances, the modulation frequency is additionally modulated with the frequency $f = 10$ kHz in the range f_{dev}=(5–500 kHz) and then lock-in detection is used at the frequency f. The parameters of such additional modulation have been optimized in a way that the registered resonances have minimal width at the maximum contrast. With

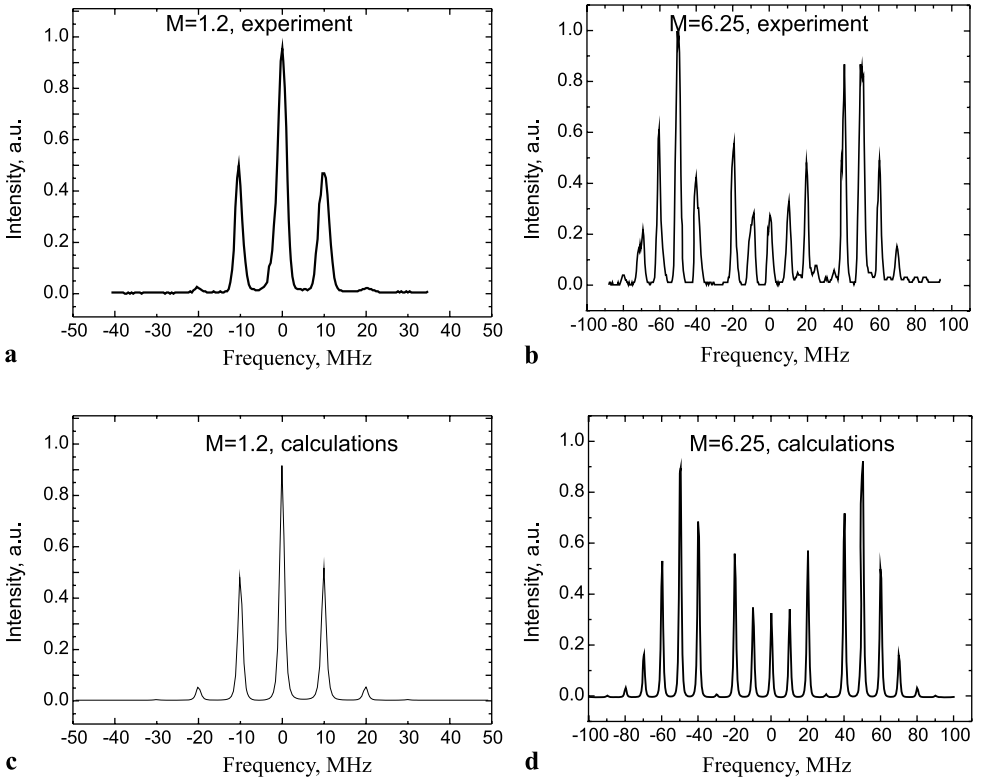

Fig. 7 Experimental (**a**), (**b**) and corresponding theoretical (**c**), (**d**) spectra of FM radiation for $M = 1.2$–6.25. All *plots* are normalized to 1 in their maximum

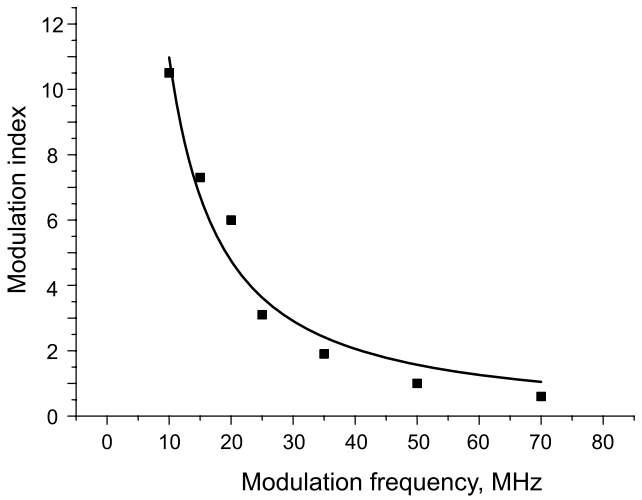

Fig. 8 Typical dependence of the FM modulation index M of the semiconductor laser radiation vs the modulation frequency Ω_{mod}. The amplitude of the generator voltage, which creates modulation of the laser diode current, was maintained constant. Solid line shows approximation by the function $M = A/(\Omega_{\text{mod}}/(2\pi \times 1\ \text{MHz}))^B$, where $A = 1.7(6) \times 10^2$ and $B = 1.21(14)$ are the approximation parameters

this, the value f_{dev} is on the order of the resonance width. Dark resonances have dispersion form because at the exit of the lock-in detector a signal is formed that is proportional to the frequency derivative from the spectral response of the atomic system. This, however, is valid only until the spectral spacing between dark resonances of the nearest order k and $k + 1$ is bigger than the value $k \times f_{\text{dev}}$, which defines the swings range of the difference frequency of all the mode pairs in the incident spectrum of the laser field that excite the resonance of the order k. For large values of k of a pair of modes, a few resonances of the higher order will be excited simultaneously, which will lead to increasing their amplitudes in the registered spectrum.

This is, however, valid only until the frequency shift in between the CPT-resonances of the neighboring orders k and $k + 1$ equal to ω_{12}/k^2 remains larger than the value of $k \times f_{\text{dev}}$, which defines the characteristic amplitude of the difference frequency sweep of the pair of modes in the laser spectrum that excite the resonance of the kth order. For large values of k, one pair of modes will excite several resonances of the higher orders simultaneously, which will lead to the change in their amplitude. The maximal order of the experimentally registered resonance for which one can use the theoretical model developed by us is given by the following relationship:

$$k_{\max} \approx \sqrt[3]{\frac{\omega_{12}}{f_{\text{dev}}}} = \sqrt{\frac{\Omega_{\text{mod}}}{f_{\text{dev}}}}. \tag{13}$$

Two different sample cells containing Rb vapor were used in the experiments. The first (we will call it the "vacuum" cell) is 20 cm in length and contains pure Rb vapor; residual vacuum is not less than 10^{-2} mbar. It was used for testing the theoretical model suggested by us. In this cell,

spectral width of the upper level (6 MHz) becomes less than the typical modulation frequency Ω_{mod} and each mode of FM-field selectively excites the resonance transitions of the respective velocity groups, which allow us not to take into account interference of the Zeeman sublevels of the system, and significantly simplify the calculations.

The width of the coherent dark resonances essentially depends on the buffer gas pressure [21, 27, 30]; therefore, for the registration of such narrow resonances (for the magnetometry purposes), we used another cell with the buffer Kr gas (in the following we will simply call it the "buffer cell") with the buffer gas pressure of about 70 Pa measured at the cell production. For increasing the absorption at the resonance transition, the buffer cell was heated up to the temperatures 60÷75°C with the use of a bifilar wire; the influence of the applied magnetic field was minimal.

The width of the dark resonances from a buffer gas cell is determined first of all by the inhomogeneity of the magnetic field in the cell and due to the contribution of the quadratic Zeeman effect [29]. At the magnetic field larger than 10 G, it is possible to resolve the components of the resonance, and their width for $B = 14$ G is approximately equal to 15 kHz. For the vacuum cell, the typical width is about 200 kHz.

6 Modeling spectra of FM spectroscopy of coherent dark resonances in a vapor of Rb atoms

For detailed comparison of our theoretical calculations with experimental data, we distilled a respective set of parameters from various experimental data in experiments with Rb (with and without buffer gas) and vacuum cells. Dipole moments d of the employed transitions were taken from [31], Rabi frequencies g and decay rates γ were calculated using the equations:

$$g = dE/\hbar, \qquad \gamma = 4d^2\omega^3/3\hbar c^3,$$

where m and e are the mass and charge of the electron, respectively, c is the speed of light and ω is the transition frequency. In an experiment with the constant magnetic field, the field strength was 14 G and the Zeeman splitting calculated with the formula $\Delta = egH/2mc$ was equal to 10 MHz for the level $5^2S_{1/2}(F = 2)$.

Using the mathematical technique outlined in Sect. 4, we calculated the absorption spectra of Rb atoms in a frame of a three-level model taking into account additional modulation of the frequency Ω_{mod} and an additional decay channel, corresponding to the respective RB atoms alone, as well as the buffer Kr gas at different excitation conditions:

- when the magnetic field was fixed and the modulation frequency Ω_{mod} was scanned;
- when the modulation frequency is fixed and the magnetic field if scanned.

Taking into account additional modulation of the frequency Ω_{mod} with deviation f_{dev} and modulation frequency f in the master equations does not affect the detected dependencies because this additional modulation frequency is much bigger than the reverse time of the dark resonances formation. Note also that we took into account in all our calculations the modulation index dependency vs the modulation frequency (see Sect. 5), which is important for the spectra calculations at the fixed magnetic field.

6.1 Case of the fixed magnetic field

In this subsection, we will consider a case when the applied magnetic field is fixed, i.e., the Zeeman splitting does not change, but we scan the modulation frequency Ω_{mod}.

Both experimental and calculated spectra of the dark resonances in a vacuum cell are shown in Fig. 9(a), (b). A separate scale on the experimental figure shows values of the FM index M, obtained from the measurement and calculations using formula (12) (for this figure, $A = 54$, $B = 1.21$). Figure 9(c) shows the dependency of the resonances width versus their order k. It can be easily seen that the experimental and theoretical graphs qualitatively fit each other. Some discrepancy between experimental data and theoretical calculations for the resonances with $k > k_{\max} = 4$ can be explained by the reasons mentioned above (Sect. 5).

The dependence of the resonances widths versus their order k shows that for the small values of orders one can see significant decrease of the width of the resonances with the increase of their order, which tends to be saturated. By all appearance, this saturation is due to the modulation registration technique because at the frequency modulation the width of the observed resonance cannot be less than the modulation amplitude, i.e., the value of f_{dev}.

6.2 Case of the fixed modulation frequency

Figure 10 shows both experimental and calculated dependencies of the lock-in detector signal versus the magnetic field B at the fixed modulation frequency $\Omega_{\text{mod}} = 4$ MHz. In this case, a qualitative agreement between the experiment and theory in connection with the amplitudes of the resonances for $k \leq k_{\max} = 4$ is also observed. However, the width of the experimentally registered resonances of the higher orders is significantly higher than those of the respective resonances in the theory. Moreover, this difference grows with increasing k. Figure 10(d) shows that the resonances' width is directly proportional to their order and, respectively, to the magnetic field strength. This means that the resonance width is determined, first of all, by the inhomogeneity of the magnetic field inside the sample cell, which, in its turn, depends on the dimensions of the cell and the solenoid and their relative position, whereas in our theoretical analysis the magnetic field was assumed homogeneous.

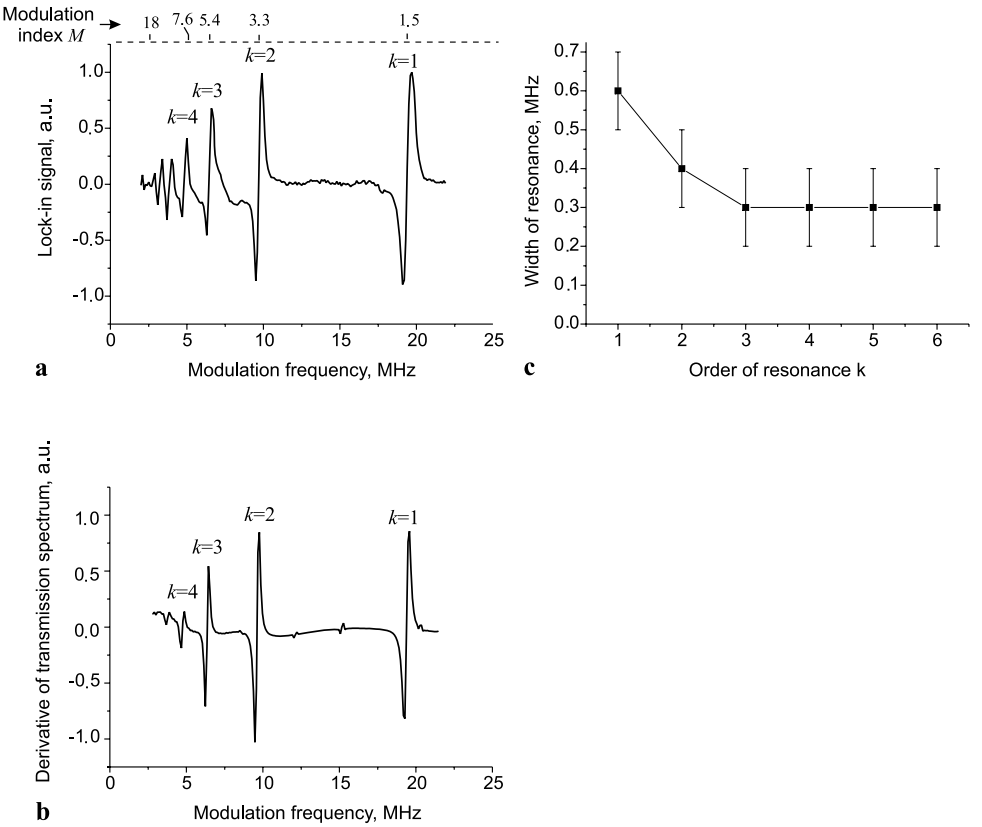

Fig. 9 (**a**) Experimental spectrum of coherent dark resonances from a cell with a vapor of ^{87}Rb atoms taken at the fixed magnetic field $B = 14$ G by scanning the modulation frequency at the following parameters: deviation $f_{\text{dev}} = 200$ kHz, intensity of the incident FM-light $P \approx 500$ μW, and the detector time constant $\tau = 3$ ms. Modulation index M for the most prominent resonances in the spectrum is shown on the top of the figure. (**b**) Theoretical calculations for the derivative of the transmission light from the sample cell for the mentioned above experimental parameters. (**c**) Dependence of the resonances widths versus their orders k (the resonances are labeled with the respective orders which reach $k_{\max} = 4$ at the given experimental parameters)

Experiments with the fixed modulation frequency are advantageous to those with the fixed magnetic field by the fact that the FM index M does not change during the measurement process, which significantly simplifies the theoretical interpretation.

7 Feasibility of using FM spectroscopy of coherent dark resonances in application to magnetometry

In this section, we will analyze both experimental data and our theoretical model for the FM spectroscopy of coherent dark resonances in application to magnetometry. We start with the fact that the frequencies of the observed dark resonances are connected with the magnetic sublevels splitting and completely determined by the magnetic field strength B, which is applied to the sample cell with a vapor of Rb atoms by the Breit–Rabi formula that gives for the nth order resonance (in a linear on the magnetic field approximation) the following frequency [32]:

$$\Omega_n \approx \frac{1}{n} 1.399 \text{ MHz/G} \cdot B.$$

Therefore, measuring of the constant magnetic field is reduced to the measuring of the frequency of any of the registered dark resonances under the condition that we know its order. The latter can be easily determined either by measuring several registered resonances or by measuring first the magnetic field with the help of a more coarse detector.

Let us estimate the resolving power for the magnetic field measurements, which can be attained in our experimental setup. For the magnetometry applications, using the buffer cell is preferable because the spectral width of the coherent dark resonances in the presence of a buffer gas is significantly narrower [19]. Figure 11 shows a fundamental ($k = 1$) dark resonance, which was detected in a buffer cell with buffer gas at the constant magnetic field with $B \approx 14$ G. Due to the quadratic Zeeman effect, the resonance at the frequency $\nu \approx 19.55$ MHz is split into three components [29]. For each of them, the whole width at the half-maximum is equal to $\Delta\nu \approx 20$ kHz and the signal-to-noise ratio $S/N \approx 150$. The registration of the signal was made at the time constant of the lock-in amplifier $\tau = 3$ ms. Because the frequency of the central component is proportional to the magnetic field induction, the resolution for magnetometry applications (i.e., the minimal change of magnetic induction, which can be measured) can be estimated as:

$$\frac{\sigma_B(\tau = 3 \text{ ms})}{B} \approx \frac{1}{Q}\frac{1}{S/N} = \frac{\Delta\nu}{\nu}\frac{1}{S/N} \approx 7 \times 10^{-6}, \qquad (14)$$

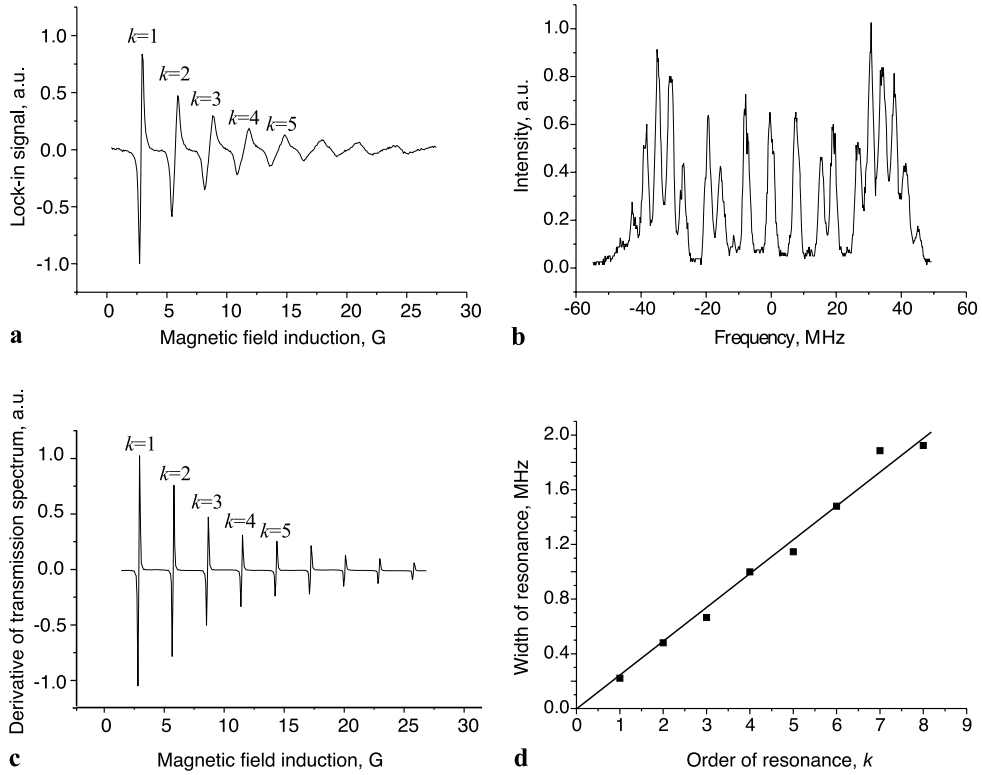

Fig. 10 (**a**) Experimental spectrum of coherent dark resonances from a cell with a vapor of ^{87}Rb atoms taken at the fixed modulation frequency $\Omega_{\text{mod}} = 4$ MHz by scanning magnetic field B at the following parameters: FM index $M = 10$, deviation $f_{\text{dev}} = 200$ kHz, intensity of the incident FM-light $P = 64$ mkW, and the lock-in detector time constant $\tau = 10$ ms. (**b**) Spectrum of the FM incident light, which is used for determination of the modulation index M. (**c**) Theoretical calculations for the derivative of the transmission light from the sample cell for the mentioned above experimental parameters and the following calculation parameters: Rabi frequencies $g_{13} = g_{23} = 1$, $M = 4$, $R = 4$, $\gamma_{13} = \gamma_{23} = 1$, $\Omega_{\text{mod}} = 4$, and $\Gamma = 3$. (**d**) Dependence of the resonances widths versus their orders k (the resonances are labeled with the respective orders which reach $k_{\max} = 4$ at the given experimental parameters)

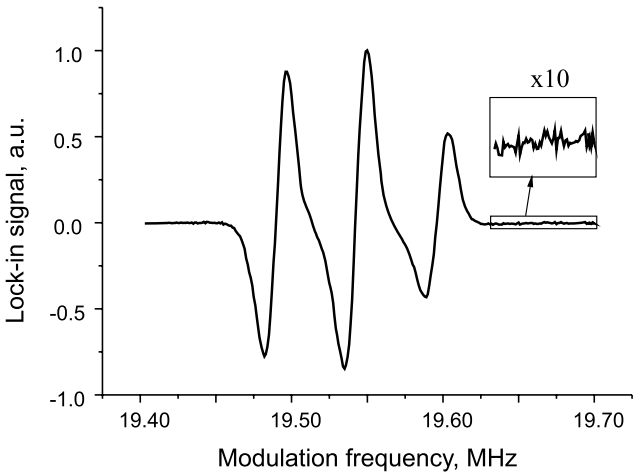

Fig. 11 Spectrum of the dark resonances taken from a vapor of Rb atoms in a buffer gas at the constant magnetic field. All resonances are split into three components due to the quadratic Zeeman effect. The magnetic field induction was roughly 14 G, the power of the pumping laser field $P = 140$ μW, and the synchronous detector time constant $\tau = 3$ ms

where $Q = \nu/\Delta\nu \approx 980$ is the resonance factor. For the magnetic field $B = 14$ G, the uncertainty $\sigma_B(\tau = 3\text{ ms}) \approx 9 \times 10^{-5}$ G.

Note that similar results were obtained earlier for Cs [14].

The maximal magnetic field strength which can be measured by the above described method is determined by the maximal frequency with which the diode laser radiation can be modulated efficiently. It equals to a few GHz, which immediately gives us the maximal possible measured magnetic field strength of about a few fractions of a tesla for the measurements taken for the first order of the resonance. Using, for example, 10th order of the resonance for the same measurements allows measurements of the magnetic field strengths of a few tesla. With this one can expect that the width of the resonances at switching from fractions to a few T will not be changed at the constant FM index and the intensity of the FM laser field [33]. Therefore, the absolute resolving power of this method is defined only by the signal-to-noise ratio.

Weak magnetic fields which cause the Zeeman splitting of the magnetic sublevels on the order of $\Delta\nu$ can be measured on a background of a larger, stable and known mag-

netic field, but not separately, because in this case there are no limitations due to the difficulty in registration of the coherent dark resonance with the frequency comparable with its own spectral width or even smaller. With this measurement technique, the absolute resolving power for the magnetic field measurements will be the same as for the larger field.

The limiting relative accuracy of the magnetometer (i.e., the maximal discrepancy between the measured value and its real value) is defined by the accuracy with which g-factors that are included into the proportionality coefficient between B and ν are known. Nowadays, it is approximately 2×10^{-6} [14, 34].

8 Conclusion

In conclusion, we made a detailed analysis and a comparison of the experimental data obtained with the FM laser spectroscopy for the D_1 line in ^{87}Rb atoms and theoretical calculations based on the model developed by us earlier [12, 13]. For this, our simple model was extended on the case of a real multilevel atom.

In the experiment, we measured dark resonances at the Zeeman sublevels of the transition $5^2S_{1/2}(F=2) \leftrightarrow 5^2P_{1/2}(F=1)$ in ^{87}Rb in transmission spectra under constant magnetic field. Simultaneously, the FM index was measured with the help of Fabri–Perot interferometer. FM spectra were registered either (i) by scanning the modulation frequency at the fixed magnetic field or (ii) by scanning the strength of the magnetic field at the fixed modulation frequency. The spectra obtained both these ways are in a good agreement with the theoretical model we had developed.

The feasibility of using FM spectroscopy of dark resonances for optical magnetometry was also discussed. The estimated attainable relative resolving power for measuring the strength of a magnetic field B in the range from 10 G to 100 G is equal to $\sigma_B/B \approx 7 \times 10^{-6}$ for the measuring time $\tau = 3$ ms in a cell of Rb atoms with a buffer gas. We also evaluated the working range for the considered magnetometer.

Acknowledgements This work has been supported by the grant No. 08-07-00127-a of the Russian Foundation for Basic Research, Presidential grants MK-1912.2008.2 and MD-887.2008.2, and the Russian Science Support Foundation grant.

References

1. S. Knappe, V. Velichansky, H.G. Robinson, J. Kitching, L. Hollberg, Rev. Sci. Instrum. **74**(6), 3142 (2003)
2. M. Fleischhauer, M.O. Scully, Phys. Rev. A **49**, 1973 (1994)
3. C.M. Caves, Phys. Rev. D **23**, 1693 (1981)
4. O.A. Kocharovkaya, Ya.I. Khanin, Sov. JETP Lett. **48**, 630 (1988)
5. S. Ospelkaus, A. Pe'er, K.-K. Ni, J.J. Zirbel et al., Nat. Phys. **4**, 622 (2008)
6. B. Julsgaard, J. Sherson, J.I. Cirac, J. Fiuraek, E.S. Polzik, Nature **432**, 482 (2004)
7. C.H. van der Wal, M.D. Eisaman, A. Andre, R.L. Walsworth, D.F. Phillips, A.S. Zibrov, M.D. Lukin, Science **301** (2003)
8. P.D.D. Schwindt, S. Knappe, V. Shah, L. Hollberg, J. Kitching, L.-A. Liew, J. Moreland, Appl. Phys. Lett. **85**, 6409 (2004)
9. G. Bison, R. Wynands, A. Weis, Appl. Phys. B **76**, 325 (2003)
10. A. Serebrov et al., J. Res. Natl. Inst. Stand. Technol. **110**, 185 (2005)
11. G.E. Hall, S.W. North, Annu. Rev. Phys. Chem. **51**, 243 (2000)
12. J. Vladimirova, B. Grishanin, V. Zadkov, V. Biancalana, G. Bevilacqua, Y. Dancheva, L. Moi, J. Exp. Theor. Phys. **103**, 528 (2006)
13. Yu. Vladimirova, B. Grishanin, V. Zadkov, V. Biancalana, G. Bevilacqua, Y. Dancheva, L. Moi, Laser Phys. Lett. **3**, 427 (2006)
14. Ch. Andreeva, G. Bevilacqua, V. Biancalana, S. Cartaleva, Y. Dancheva, T. Karaulanov, C. Marinelli, E. Mariotti, L. Moi, Appl. Phys. B **76**, 667 (2003)
15. G. Alzetta, A. Gozzini, L. Moi, G. Orriols, Nuovo Cimento B **36**, 5 (1976)
16. E. Arimondo, in *Progress in Optics*, vol. 35, ed. by E. Wolf (Elsevier, Amsterdam, 1999), p. 257
17. S.E. Harris, J.E. Field, A. Imamoglu, Phys. Rev. Lett. **64**, 1107 (1990)
18. M. Lukin et al., Opt. Lett. **4**, 295 (1998)
19. S. Brandt, A. Nagel, R. Wynands, D. Meschede, Phys. Rev. A **56**, 1063 (1997)
20. M. Erhard, H. Helm, Phys. Rev. A **63**, 043813 (2001)
21. A.V. Tachenachev, A.M. Tumaikin, V.I. Yudin, M. Stahler, R. Wynands, J. Kitching, L. Hollberg, Phys. Rev. A **67**, 033810 (2003)
22. A.V. Tachenachev, A.M. Tumaikin, V.I. Yudin, M. Stahler, R. Wynands, J. Kitching, L. Hollberg, Phys. Rev. A **69**, 024501 (2004)
23. Yu.V. Vladimirova, B.A. Grishanin, V.N. Zadkov, N.N. Kolachevskii, A.V. Akimov, N.A. Kisilev, S.I. Kanorskii, J. Exp. Theor. Phys. **96**, 629 (2003)
24. J. Belfi, G. Bevilacqua, V. Biancalana, Y. Dancheva, L. Moi, J. Opt. Soc. Am. B **7**, 1482 (2007)
25. P.D.D. Schwindt, S. Knappe, V. Shah, L. Hollberg, J. Kitching, L.-A. Liew, J. Moreland, Appl. Phys. Lett. **26**, 6409 (2004)
26. A.V. Taichenachev, A.M. Tumaikin, V.I. Yudin, G. Nienhuis, Phys. Rev. A **69**, 033410 (2004)
27. S.A. Zibrov, V.L. Velichansky, A.V. Tachenachev, V.I. Yudin, J. Exp. Theor. Phys. Lett. **82**, 534 (2005)
28. A.V. Akimov, A.N. Matveev, A.V. Sokolov, E.O. Tereshenko, D.A. Kondratjev, V.N. Sorokin, S.I. Kanorsky, N.N. Kolachevsky, J. Raman Spectrosc. **37**, 712 (2006)
29. A.V. Tachenachev, V.I. Yudin, A.Yu. Samokotin, A.V. Akimov, A.V. Sokolov, V.N. Sorokin, N.N. Kolachevsky, JETP Lett. **88**, 355 (2008)
30. E. Arimondo, Phys. Rev. A **54**, 2216 (1996)
31. D.A. Steck, Rubidium 87 D line data, the current version of this document is available at http://steck.us/alkalidata
32. A. Corney, *Atomic and Laser Spectroscopy* (Clarendon, Oxford, 2006)
33. A.V. Akimov, A.N. Matveev, A.V. Sokolov, S.I. Kanorsky, N.N. Kolachevsky, G.Yu. Pakhutin, V.N. Sorokin, J. Russ. Laser Res. **25**, 239 (2004)
34. R. Wynands, A. Nagel, Appl. Phys. B **68**, 1 (1999)